Available online at www.sciencedirect.com
ScienceDirect
Journal of Nuclear Materials 376 (2008) 38–46
journal of nuclear materials
www.elsevier.com/locate/jnucmat

Fatigue testing of metallurgically-bonded EBR-II superheater tubes

T.C. Totemeier [a,1], D.M. Wachs [b], D.L. Porter [b,*], N. Kisohara [c]

[a] Alstom Power Inc., 2000 Day Hill Road, Windsor, CT 06095, USA
[b] Idaho National Laboratory, P.O. Box 1625, MS 6188, Idaho Falls, ID 83415-6188, USA
[c] Japan Atomic Energy Agency (JAEA), FBR System Design Group, 4002 Narita, Oarai, Ibaraki Pref., 311-1393, Japan

Received 27 November 2007; accepted 5 February 2008

Abstract

Fatigue crack growth tests were performed on 2¼Cr–1Mo steel specimens machined from ex-service experimental breeder reactor-II (EBR-II) superheater duplex tubes. The tubes had been metallurgically-bonded with a 100 μm thick Ni layer; the specimens incorporated this bond layer. Fatigue crack growth tests were performed at room temperature in air and at 400 °C in air and humid Ar; cracks were grown at varied levels of constant ΔK. In all conditions the presence of the Ni bond layer was found to result in a net retardation of growth as the crack passed through the layer. The mechanism of retardation was identified as a disruption of crack planarity and uniformity after passing through the porous bond layer. Full crack arrest was only observed in a single test performed at near-threshold ΔK level (12 $MPa\sqrt{m}$) at 400 °C. In this case the crack tip was blunted by oxidation of the base steel at the steel–nickel interface.
Published by Elsevier B.V.

1. Introduction

The experimental breeder reactor-II (EBR-II), a sodium-cooled fast reactor, was operated for over 30 years. The evaporators and superheaters used in the EBR-II were developed to meet the unique challenges associated with sodium–water heat exchange. After 30 years of operation they provide a unique source of plant-aged materials that can be used to study potential mechanical property degradation as it may apply to current and future power plant design and operation.

The steam generator system of the EBR-II consisted of a conventional steam drum, eight shell-and-tube evaporators (steam generators), and two shell-and-tube superheaters [1]. The superheaters were of the counter-flow type with once-through flow of sodium and steam. Operating temperatures were approximately 468 °C (inlet) and 428 °C (outlet) on the sodium side, and 304 °C (inlet) and 438 °C (outlet) on the steam side. Safe operation of the plant required that sodium–steam contact be prevented; the heat exchanger tubes were designed such that tube failure would be a very low probability event, without compromising overall heat exchanger efficiency. Assuming that it would be much less likely to propagate a crack through a tube-in-tube than a single tube, duplex (tube-in-tube) heat exchanger tubes were used.

Steam tubes in the EBR-II superheaters were constructed from 2¼Cr–1Mo steel (ASME SA-213, Grade T22). Two types of duplex tube construction – mechanical and metallurgically-bonded – were used, one type for each superheater. The tubes were mechanically-bonded by drawing them simultaneously over a mandrel and through a die to create a large contact pressure between the inner and outer tubes. In service, however, the radial bonding stresses relaxed, creating gaps at the tube interface, poor heat-transfer through the tube, and poor overall performance of the superheater [2]. In 1981, the superheater with mechanically-bonded tubes was removed and replaced with an evaporator unit with metallurgically-bonded tubes (eight evaporator units in the EBR-II steam system were built to the same designs as the superheater units). A post-service examination of the mechanically-bonded tubes

* Corresponding author. Tel.: +1 208 533 7659; fax: +1 208 533 7996.
E-mail address: douglas.porter@inl.gov (D.L. Porter).
[1] Formerly with the Idaho National Laboratory, USA.

0022-3115/$ - see front matter Published by Elsevier B.V.
doi:10.1016/j.jnucmat.2008.02.004

Table 1
Approximate bond layer temperatures

Location	Average temperature (°C)	Temperature gradient across tube wall (°C)
Lower region	453	30
Upper region	366	124

from the discarded superheater unit was performed which verified the formation of gaps between the inner and outer tubes [3].

Metallurgically-bonded tubes performed well through the reactor lifetime. These tubes were created by plating the contact surfaces of the inner and outer tubes with nickel prior to assembly of the duplex tubes. The outer surface of the inner tube was electroplated with nickel from a Watts bath to 100 μm thickness, and the inner surface of the outer tube was electroless plated with nickel to approximately 15 μm thickness. The plated tubes were drawn together using the same procedure as the mechanically-bonded tubes, then annealed and heat treated by three successive passes through a tube furnace at 926, 1121, and 760 °C. The feed rate of the tubes through the furnace was such that each tube spent approximately 30 min at each temperature. Heat treatment at these conditions corresponds to a normalized-and-tempered condition for 2¼Cr–1Mo steel [4]. Drop-weight impact tests on miniature Charpy V-notch test specimens machined from the bonded tubes verified the crack-arresting ability of the bond layer under impact conditions at 25 and 449 °C [5].

To assess the condition and performance of the metallurgically-bonded tubes after 30 years of service, four tube sections were removed from EBR-II superheater number 710. Windows were cut in the upper and lower region of the superheater; shell and tube sections were removed from each region. The operating temperatures of the upper and lower tube sections have been calculated and are listed in Table 1.

This paper reviews the post-service metallurgical examination and testing of the tubes previously reported [6]. Then, it details new results concerning fatigue crack growth tests that were performed to assess the crack-arresting ability of the nickel interlayer in cyclic loading conditions after long-term service. Fatigue crack growth tests were performed on bonded tube specimens in air at room temperature and 400 °C, and in a humid Ar environment at 400 °C.

2. Post-service material characterization

The duplex tubes were constructed from 2¼Cr–1Mo steel produced to ASME specification SA-213, Grade T22. The exact chemistry of the heat used to create the tubes studied is unavailable. Metallographic examinations of the post-service tubes were presented in detail previously [6]. The exams showed that the overall condition of the metallurgically-bonded superheater tubes after 30 years of service was good. No excessive corrosion occurred on either the steam or sodium sides of the tubes, and the duplex tubes remained bonded. Diffusion of Fe and Cr into the Ni bond layer clearly occurred, and this led to pore formation in the steel adjacent to the bond layer.

Fig. 1 is an overview of the bond layer structure in a tube removed from the upper area of the superheater. The plane observed is normal to the long axis of the tube; the outside diameter of the tube is oriented to the top of the image. The nickel bond layer is clearly apparent as an unetched band in the center. The 2¼Cr–1Mo tubes still show a tempered bainite structure.

Fig. 2 shows the results of an energy-dispersive X-ray spectroscopy (EDS) line scan across the bond layer. As demonstrated in a previous examination of these interfaces [6], Fe and Cr have diffused into the Ni layer. Although values are not shown in the figure, standardless, semi-quantitative analysis shows approximately 7–8 wt%. Fe in the center of the interlayer and 40–45 wt% at the edges. Little Ni appears to have diffused into the base steel. Analysis of the dark grey phase (Fig. 1) reveals it to be a Ni–Ni_3P eutectic with an overall P content of approximately 10 wt%. These latter data provide added information to that given in Ref. [6].

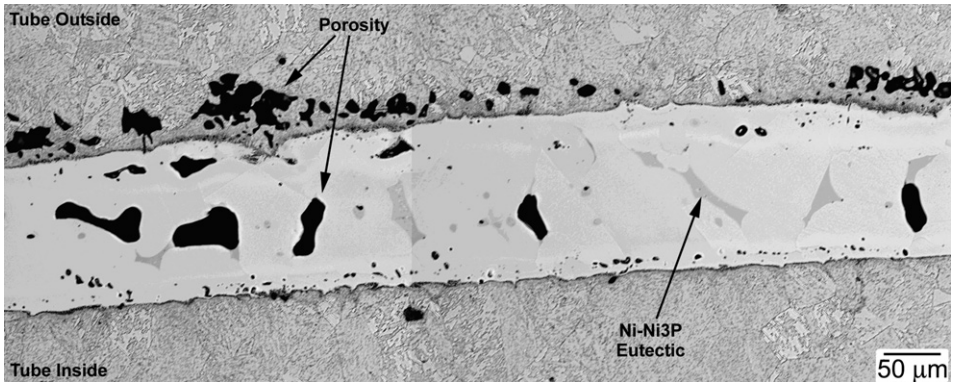

Fig. 1. Polished and etched cross-section (normal to tube axis) of the metallurgical bond in an EBR-II superheater tube after 30 years of service (upper tube section).

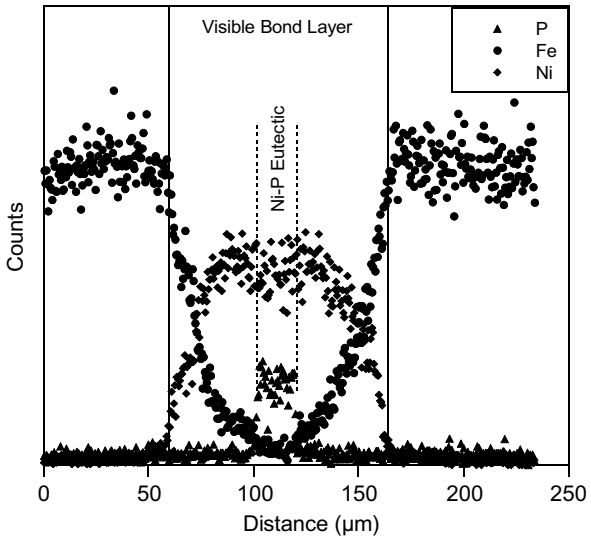

Fig. 2. Results of EDS linescan across bond layer for Ni, Fe, and P. Line traverses dark gray Ni–P eutectic in center of bond layer.

3. Impact testing

The original intent of using duplex tubes was to reduce the risk of cracks propagating through the tubes and allowing direct steam–sodium contact. The metallurgically-bonded tubes were shown previously to continue to perform this function under the loading conditions experienced in an impact test, e.g., high strain rates and gross overall deformation, even after 30 years of exposure [6]. With the exception of one specimen at −50 °C (a temperature which would not be realistically occur in service), all impact test specimens failed in a ductile manner with the crack arrested by the bond layer. No embrittlement of the steel was observed (a potential issue with 2¼Cr–1Mo steels [4]), nor had brittle intermetallic phases formed by interdiffusion [6].

4. Fatigue crack growth testing

In this present study fatigue crack growth (FCG) testing of specimens machined from bonded tubes was performed to assess the ability of interlayer to arrest or retard the growth of fatigue cracks propagating through duplex tubes. The primary postulated cause of fatigue cracking in steam generator tubing similar to that used in EBR-II is departure from nucleate boiling (DNB) events which cause thermal oscillations on the steam side of the tube wall. The resistance of the bond layer to fatigue crack growth was assessed by growing cracks through the bond layer at a range of constant ΔK values. Values in the near-threshold, Paris, and accelerating growth regimes were chosen to determine the behavior over the broadest range of conditions. Tests were performed at room temperature and at the 400 °C approximate service temperature.

4.1. Test procedures

Rectangular bend-bar specimens with overall dimensions identical to the impact specimens were machined from the ex-service, bonded tubes and used for FCG testing (Fig. 3). Instead of 30° V-notches, 0.8 mm deep starter notches were cut using a jeweler's saw (0.5 mm width) or by electro-discharge machining with a 0.5 mm wire. Notches were made such that crack growth occurred from both inside to outside and outside to inside directions to observe any differences in crack growth behavior caused by the porosity formation on one side of the bond layer. As described below, no difference was found.

Tests were performed in 3-point bending on an Instron 8501 servo-hydraulic test machine; the requirements of ASTM test standard E 647-00 were followed to the extent possible given the small specimen sizes. A small servo valve and a 5 kN load cell were used to accurately generate and measure the low forces (~50–300 N) needed for testing the small specimens. For tests at 400 °C, the specimens and loading platens were heated in a box-type resistance furnace; the platens and loading rods were machined from a high-strength nickel alloy and stainless steel, respectively. Alumina rod was used for loading pins to electrically insulate the specimen. A type K thermocouple was spot-welded to the specimen to monitor temperature.

For some tests at 400 °C a humid Ar atmosphere was created in the furnace as a crude steam environment simulation by flowing ultra-high-purity Ar through a bubbler containing distilled water at room temperature. The humidified Ar was then piped into the furnace via a stainless steel tube whose outlet was adjacent to the specimen. The interior of the box furnace was nominally sealed by stuffing gaps with alumina fiber insulation. Ar was continually flowed into the furnace during testing at a low flow rate (visibly bubbling, not measured).

Room temperature tests were performed in air with a sinusoidal waveform at a nominal cyclic frequency of 20–30 Hz. The frequency was lowered (to a minimum of 1 Hz) during periods of rapid crack growth for better control. An R ratio ($=K_{min}/K_{max}$) of 0.1 was used for all tests with the exception of test JNC-24, as described below. At 400 °C, crack initiation was performed at 20 Hz; cracks were grown at this frequency to ~1.15 mm length. At this point the frequency was lowered to 1 Hz and all subsequent

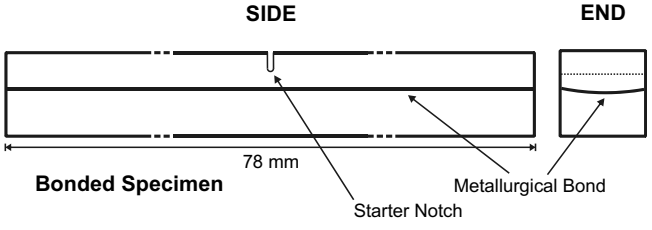

Fig. 3. Schematic diagram of fatigue crack growth test specimen; end dimensions are 3.8 mm square.

loading occurred at this frequency, which roughly corresponds to the frequency of thermal loading caused by departure from nucleate boiling (DNB) events [7,8].

Cracks were grown at constant ΔK; three levels were used: 10–12 MPa$\sqrt{m}$ (near-threshold), 15 MPa$\sqrt{m}$ (Paris regime), and 20 MPa$\sqrt{m}$ (accelerating crack growth). The levels were selected based on previous results from similar material taken from the shell of the superheater [9]. Cracks were initiated from the notch at 15 to 16 MPa$\sqrt{m}$; for tests to be performed at a lower stress intensity range (i.e., near-threshold), the stress intensity was lowered to the test level after a very small (20 μm) increment of crack growth.

Crack lengths were measured during testing by the direct-current potential drop (DCPD) method. Load ranges were adjusted as the crack grew so that the ΔK level was maintained within ±0.2 MPa$\sqrt{m}$. Potential drop reading and load range were continually recorded using a computer-based test acquisition system. Cracks were typically grown to a length of 2.5–2.7 mm. The specimens were then broken after cooling in liquid N_2 to clearly demark the final fatigue crack position. Post-test fractography was performed on selected specimens using stereo light microscopy at low magnifications and scanning electron microscopy at higher magnifications. Metallographic cross-sections of a specimen in which crack arrest occurred were prepared and examined.

4.2. Results – fatigue crack growth rates

The behavior of all specimens was similar; Fig. 4 shows a typical test which was conducted at 14.5 MPa$\sqrt{m}$ with the crack growing from inside to outside (specimen JNC-22). Crack length is plotted as a function of cycles. The location of the metallurgical bond (determined from the fracture surface) is superimposed on the plot. The growth rate gradually increases as the crack grows away from the notch, reaching a constant rate of 2.2×10^{-5} mm/cycle prior to entering the bonded layer. The growth rate further increases just prior to and in the bond layer, achieving a maximum rate of 5.2×10^{-5} mm/cycle. The crack is markedly retarded for distance of 0.5 mm after the bond layer, growing at a rate of 8.9×10^{-6} mm/cycle. Near the end of the test the crack re-accelerates to a rate identical to that measured before the bond was entered, and grows at this linear rate until the test is terminated. The net retardation in crack growth in terms of number of cycles is equal to the X-axis offset of the two baseline curves, in this case about 20 000 cycles.

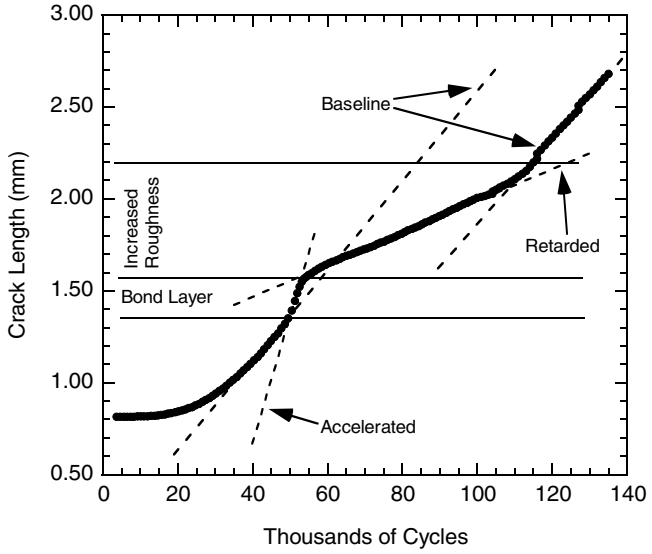

Fig. 4. Crack length versus cycles for test JNC-22, upper tube section, $\Delta K = 15$ MPa$\sqrt{m}$. Rates corresponding to those listed in Table 2 are shown as dashed lines; the location of the bond layer and zone of increased crack roughness with respect to the crack length are also shown.

Table 2 summarizes conditions for tests at room temperature and lists the growth rates measured in the different regions of each specimen as described above. Not all cracks were grown to sufficiently long lengths to measure the re-accelerated rate. The baseline rates did not vary with specimen location in the superheater (upper/lower) or crack growth direction and matched the rates obtained on 2¼Cr–1Mo shell material [9]. The amount of acceleration and retardation due to the bond layer varied from test to test but was roughly a factor of 1.5–3 for acceleration (accelerated rate divided by baseline rate) and 2–4 for retardation (post-bond retarded rate divided by baseline rate). The accelerated rate in the bond layer increased with ΔK, varying from 8×10^{-6} mm/cycle at 12 MPa$\sqrt{m}$ to 2×10^{-4} mm/cycle at 20 MPa$\sqrt{m}$.

Test JNC-24 was conducted at a higher R ratio (0.45) to observe the effect of crack closure on the acceleration and retardation behavior. Crack closure effects trend to reduce growth rates at near-threshold ΔK. Closure effects are lessened by increasing the minimum load in the cycle, i.e., by testing at a higher R ratio [10]. In this test R was limited to 0.45 by the need to keep K_{max} less than 25 MPa$\sqrt{m}$ while also keeping ΔK greater than 12 MPa$\sqrt{m}$ for comparison with previous tests. With respect to the baseline $R = 0.1$, crack growth rates were accelerated in all regions of the specimen, as expected, but the factors of acceleration and retardation were similar to previous tests. The lack of change in acceleration and retardation factors indicates that closure effects on the processes accelerating and retarding crack growth in and after the bond were minimal.

The crack growth behavior observed in air and humid Ar at 400 °C was essentially identical to that at room temperature; test conditions and results are listed in Table 3. The factors of acceleration and deceleration were similar to those at room temperature, although the growth rates at a given ΔK were slightly higher. One exception was the test conducted in air at 12 MPa$\sqrt{m}$ (JAEA-400-6), in which a full crack arrest occurred, as shown in Fig. 5. Test JAEA-400-11 was also conducted at a relatively low ΔK level (14.5 MPa$\sqrt{m}$), but in this case an order of magnitude growth rate reduction occurred instead of complete crack arrest.

Table 2
Test conditions and results for room temperature fatigue crack growth tests

Test ID	Material	Crack growth direction	ΔK (MPa $m^{1/2}$)	Baseline rate prior to bond layer (mm/cycle)	Accelerated rate before/in bond layer (mm/cycle)	Retarded rate after bond layer (mm/cycle)	Re-accelerated rate after bond layer (mm/cycle)
JNC-17	Lower tube	Outside to inside	14	2.2×10^{-5}	3.3×10^{-5}	5.2×10^{-6}	–[a]
JNC-18	Lower tube	Inside to outside	14.5	2.3×10^{-5}	3.8×10^{-5}	6.7×10^{-6}	1.6×10^{-5}
JNC-19	Upper tube	Outside to inside	14	2.3×10^{-5}	3.5×10^{-5}	7.0×10^{-6}	–[a]
JNC-20	Upper tube	Outside to inside	20	6.3×10^{-5}	2.2×10^{-4}	1.9×10^{-5}	3.8×10^{-5}
JNC-21	Upper tube	Outside to Inside	12	4.7×10^{-6}	8.2×10^{-6}	2.2×10^{-6}	–[a]
JNC-22	Upper tube	Inside to outside	14.5	2.2×10^{-5}	5.2×10^{-5}	8.9×10^{-6}	2.2×10^{-5}
JNC-23	Lower tube	Outside to inside	14.7	2.5×10^{-5}	4.0×10^{-5}	–[a]	–[a]
JNC-24	Lower tube	Outside to Inside	12[b]	1.4×10^{-5}	3.1×10^{-5}	5.2×10^{-6}	–[a]

[a] Test terminated prior to crack growth in this region.
[b] ($R = 0.45$).

Table 3
Test conditions and results for 400 °C fatigue crack growth tests

Test ID	Material, environment	Crack growth direction	ΔK (MPa $m^{1/2}$)	Baseline rate prior to bond layer (mm/cycle)	Accelerated rate before/in bond layer (mm/cycle)	Retarded rate after bond layer (mm/cycle)	Re-accelerated rate after bond layer (mm/cycle)
JAEA-400-4	Upper tube, Air	Outside to inside	14	2.8×10^{-5}	5.2×10^{-5}	6.7×10^{-6}	1.6×10^{-5}
JAEA-400-5	Lower tube, Air	Inside to outside	14.5	2.0×10^{-5}	3.5×10^{-5}	7.7×10^{-7}	–[a]
JAEA-400-6	Upper tube, Air	Inside to outside	12	2.0×10^{-5}	5.4×10^{-5}	Crack arrest	–[a]
JAEA-400-7	Upper tube, Air	Inside to outside	19	5.2×10^{-5}	1.4×10^{-4}	1.6×10^{-5}	4.5×10^{-5}
JAEA-400-10	Upper tube, Humid Ar	Inside to outside	16.5	3.6×10^{-5}	1.1×10^{-4}	1.4×10^{-5}	3.8×10^{-5}
JAEA-400-11	Upper tube, Humid Ar	Inside to outside	14.5	1.5×10^{-5}	4.3×10^{-5}	1.3×10^{-6}	–[a]

[a] Test terminated prior to crack growth in this region.

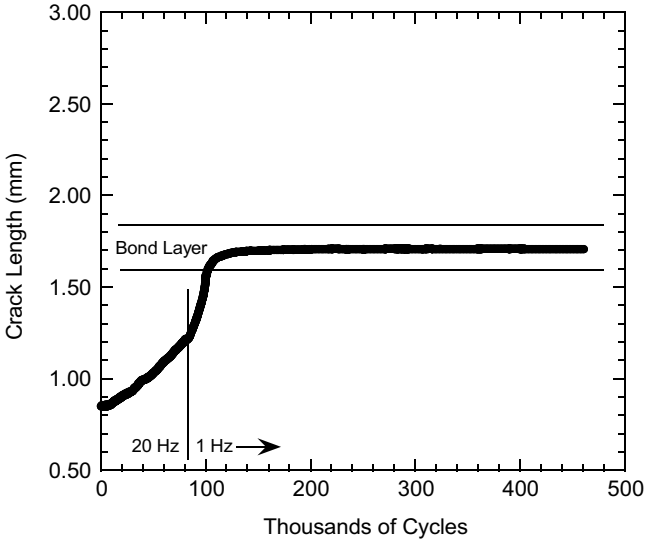

Fig. 5. Crack length versus cycles for test JAEA-400-6, upper tube section, $\Delta K = 12$ MPa$\sqrt{m}$, air environment. The crack arrests in the bond layer. Vertical line demarks change in cycling frequency from 20 to 1 Hz.

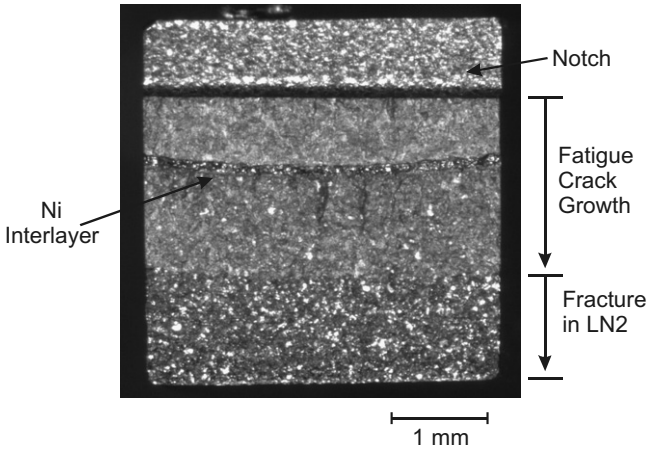

Fig. 6. Overview of specimen JNC-22 fracture surface.

4.3. Results – fractography

A light microscope overview of the fracture surface of a representative fatigue test specimen (JNC-22) is shown in Fig. 6. All other specimens showed essentially identical features, regardless of ΔK level, crack growth direction, or location within the superheater. Tests performed at 400 °C showed discoloration due to oxidation, but the fracture surface features were otherwise identical to the room temperature features described below. The EDM notch is at the top, and the fatigue crack growth area is in the center. The shiny bottom of the specimen is the area that was broken after cooling in liquid nitrogen. The metallurgical bond is clearly seen in the center of the fatigue area.

Fig. 7 shows a closer view of the fatigue area taken in the SEM. The EDM notch is again at the very top of the image, and the bond in the center. Note that the fatigue

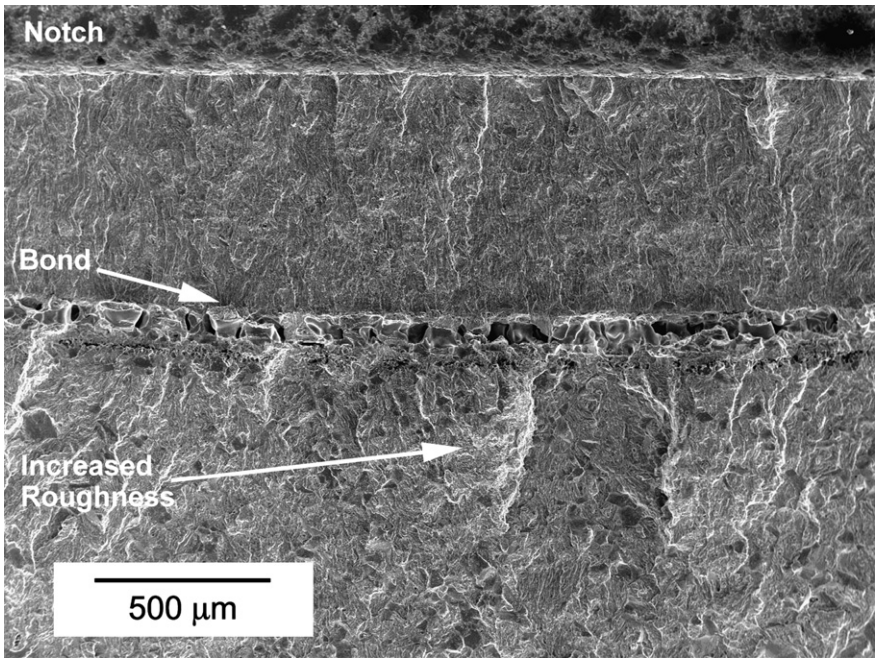

Fig. 7. SEM overview of fracture features in specimen JNC-22 showing increased roughness of the crack path after passing through the bond layer. Crack grows top to bottom.

area after the bond layer is much rougher than before; the fatigue crack has apparently re-initiated on or been diverted to several levels after passing through the bond. The increased roughness is observed for a distance that corresponds with the area of reduced crack growth rate, as indicated on Fig. 4. Similar features were observed on other specimens. A closer view of the features in the metallurgical bond is shown in Fig. 8. Areas where the crack path has followed porosity are shown by smooth, featureless surfaces; other areas show faceted features with river markings indicating brittle facture or dimples indicative of ductile rupture. The cavernous nature of some areas of the bond porosity is apparent. Fine porosity on the outside tube side of the bond is also observed.

Metallographic cross-sections prepared from the JAEA-400-6 specimen confirmed that fatigue crack arrest

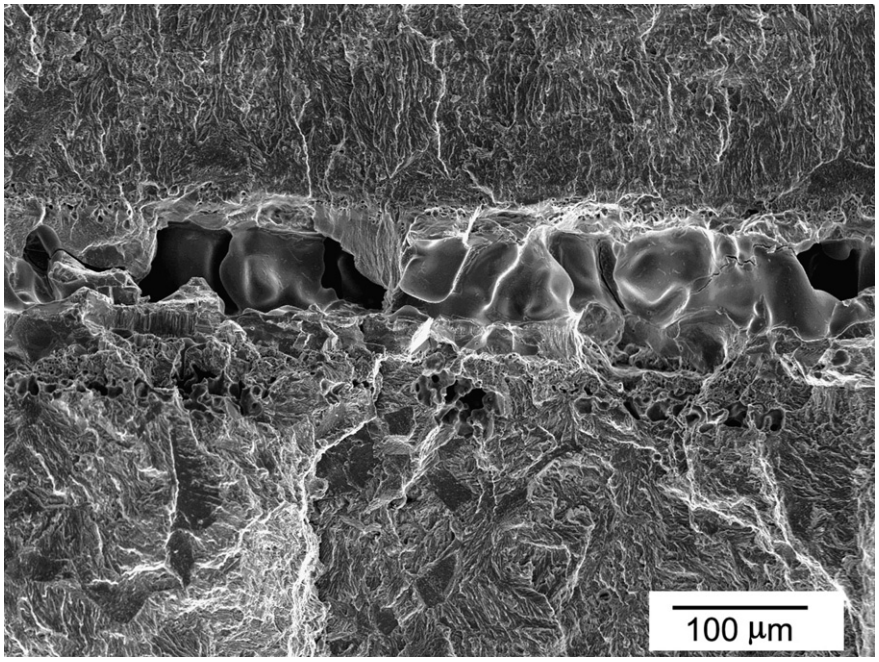

Fig. 8. Fracture features in bond area (center of image) of specimen JNC-22. Crack grows from top to bottom.

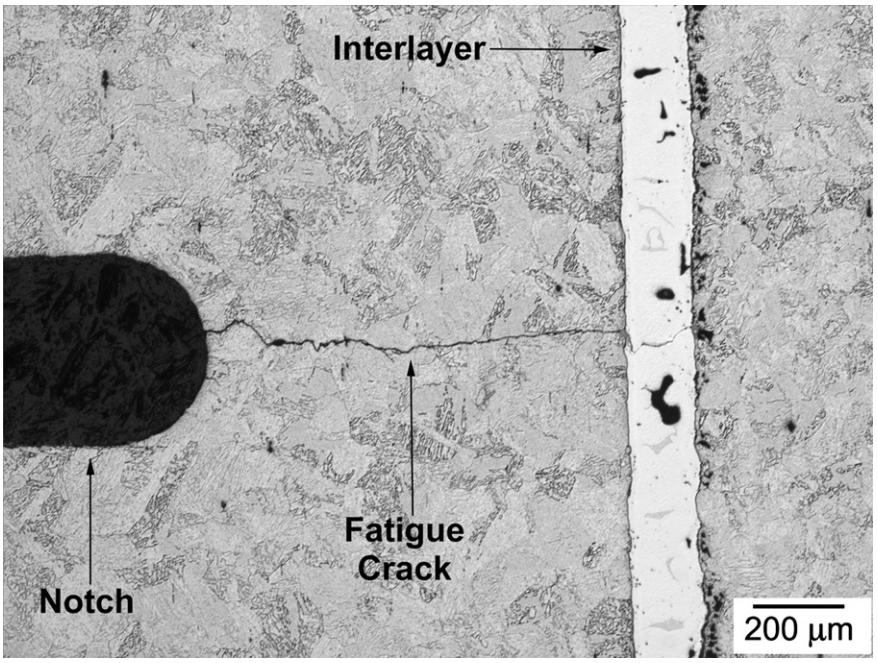

Fig. 9. Low-magnification overview of JAEA-400-6 cross-section showing fatigue crack arrested at far side of interlayer. Crack grows from left to right.

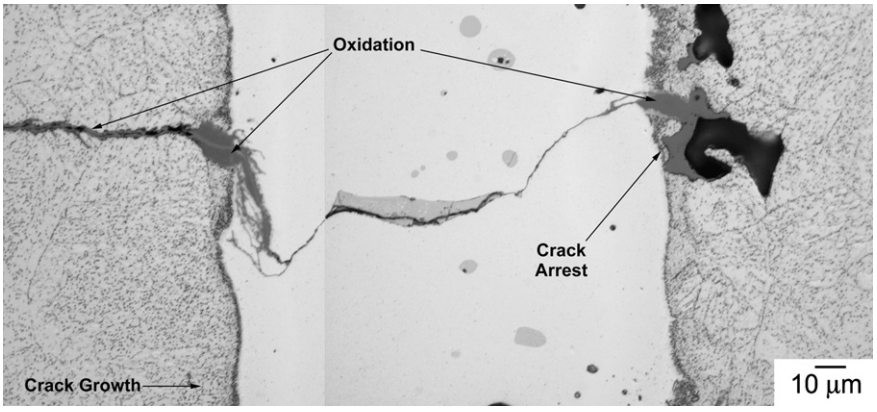

Fig. 10. Close view of interlayer in Fig. 9 showing oxidation at interlayer–steel interfaces and fatigue crack wake in steel. Crack grows from left to right.

occurred in the bond layer for this test performed at 400 °C in air. Fig. 9 shows a low-magnification overview of the crack. The starter notch is at the left and the crack propagates from the root of the notch and arrests at the far side of the bond layer, which is visible as the bright vertical band on the right side of the image. A higher magnification view of the crack tip (Fig. 10) shows oxidation at the crack tip on the right side of the bond and at the bond interface on the left side. There is little oxidation associated with the crack in the bond layer itself, but the crack wake in the steel is clearly oxidized; therefore the bond layer appears more oxidation resistant than the steel.

5. Discussion

Previously published results [6] showed that there was no apparent embrittlement of either the 2¼Cr–1Mo steel or the nickel braze. Ni–Ni_3P phases were identified in this follow-on study. The areas of Ni–Ni_3P eutectic were likely formed by partial melting of the bond layer in the high-temperature annealing step, which is above the eutectic temperature of 870 °C [11]. Their volume fraction is small, however, and they would not be expected to impair the overall ductility of the duplex tubes.

The function of the interlayer with respect to fatigue crack growth, however, was found to be different than had been observed previously, where impact-generated cracks were effectively stopped by the interface [6]. The results presented in Section 4 above indicate that at room temperature the presence of the metallurgical bond slows fatigue crack growth through the tube but does not result in complete crack arrest over the range of ΔK levels tested. The effect of the bond appears to be independent of ΔK, location within the superheater (upper versus lower tube

section), and crack growth direction (inside to outside versus outside to inside). Crack growth rates are accelerated in the bond, as expected given the high fraction of porosity in and near the bond. The retardation in crack growth rate after the bond appears to correlate with increased roughness of the fracture surface. The fact that crack growth is retarded for a significant distance after the bond indicates that the retardation effect is not simply due to re-initiation of the crack on the opposite side of the bond; this is also supported by the absence of a true arrest of the crack at any point when passing through the bond layer.

Increased surface roughness is frequently associated with crack retardation due to closure effects, especially at the low R ratio (0.1) used in the present tests [10]. Increasing the R ratio, however, did not produce a significant change in the acceleration–retardation effect of the bond layer, contrary to the expectation if a significant closure effect was present. It is believed rather that the retardation results primarily from a disruption in the planarity of the fatigue crack as it passes through the highly porous bond layer. Although the crack does not have to re-initiate, it does appear to significantly deviate out of the original propagation plane in local areas when passing through the bond layer. Such disruption in crack uniformity reduces the effective ΔK at the crack tip and slows propagation. The local deviation of the crack path likely results from the connected, cavernous nature of the porosity in the bond layer. The crack will take the path of least resistance (highest porosity) – which involves growing out of the original crack plane in different areas along the crack width. After a period of growth in the base metal the crack again becomes uniform due to the uniformity of the far-field stress, and the growth rate returns to the baseline.

The retardation effect of the interlayer at room temperature, therefore, appears to be fundamentally related to its highly porous, cavernous nature. As mentioned above, it is unclear whether porosity in the nickel layer formed during service or was present after annealing and heat treatment of the tubes. The results of metallurgical examination of the tubes prior to service are not currently available.

Similar behavior was observed at 400 °C, although a full crack arrest was observed for a low ΔK test in air. The crack arrest was likely assisted by oxidation of the base steel at the steel–bond interface, reducing ΔK by blunting the crack tip. It is important to note that it is oxidation of the steel which appears to increase propensity for arrest, not oxidation of the interlayer itself. It is not surprising that the interlayer is more oxidation resistant than the base steel, since Ni is generally more oxidation resistant than Fe [12]. It appears that the combination of reduced ΔK due to disrupted crack uniformity and blunting by crack tip oxidation led to arrest. The reduced frequency (1 Hz compared to 20 Hz) also would play a role by allowing more time for oxidation.

There was little difference in behavior between air and humid Ar at 400 °C. Specimen surfaces were similarly oxidized after testing, with perhaps slightly less oxidation in humid Ar. Due to the simplicity of the test set-up, the humid Ar environment cannot be considered to be representative of a high-pressure steam system. Tests were performed in humid Ar as a simple check to see if the behavior might be markedly different than in air, which it was not. That said, however, it is likely that the behavior in a true service environment would not be very different than that observed in the present tests, since oxidation of the steel or the Ni bond layer in steam will not be catastrophically severe, and their relative oxidation resistances will be similar.

Hence the function of the Ni bond layer as a fatigue crack arrestor appears to be limited. The layer retards crack growth over all ΔK values, but only results in crack arrest for near-threshold ΔK. It is worth repeating that the retardation function of the interlayer is only present because of the porosity defects present. A more effective interlayer for crack arrest in fatigue conditions would be one which did severely oxidize in the service environment; this would act to blunt the crack tip and arrest the crack. Crack arrest in this case would come at the expense of potentially catastrophic oxidation and reduced heat-transfer performance due to an oxidized interlayer.

6. Conclusions

Fatigue crack growth tests were performed to assess the crack-arresting ability of duplex EBR-II superheater tubes after 30 years of service exposure. Previously, impact tests on miniature Charpy V-notch specimens performed at temperatures ranging from −50 to 400 °C confirmed the ability of the nickel bond layer to arrest cracks in dynamic, high strain loading conditions [6].

The current results of the fatigue crack growth tests show that the presence of the Ni bond layer results in a net retardation of growth as the crack passes through the layer, both at room temperature and at 400 °C. The effect of the interlayer was independent of ΔK within the 12–20 $\mathrm{MPa}\sqrt{\mathrm{m}}$ range tested, location within the superheater (upper versus lower tube section), and crack growth direction (inside to outside versus outside to inside). Even though growth rates in the layer itself were accelerated with respect to the 2¼Cr–1Mo steel tube material, crack growth in the tube material after passing through the bond layer was retarded by approximately a factor of two to three due to a reduction in crack front uniformity. The crack uniformity was disrupted by the presence of large, cavernous pores in the interlayer which locally deviated the crack out of the original crack plane by offering low-resistance crack paths. At 400 °C in air, blunting of the crack tip by steel oxidation at the steel–interlayer interface led to full crack arrest for a test conducted at a near-threshold ΔK level.

Acknowledgements

The authors would like to acknowledge the assistance of T.C. Morris with metallography. This work was performed

at the Idaho National Laboratory under INL Work for Others agreement number 85Q40, funded by the Japan Atomic Energy Commission (JAEA) through the DOE Idaho Operations Office Contract DE-AC07-05ID14517.

References

[1] H.W. Buschman, W.H. Penney, M.D. Quilici, W.H. Radke, in: Proceedings of the Joint ASME/IEEE Power Generation Conference, 4–8 October 1981, St. Louis, MO (available from ASME).
[2] W.H. Penney, H.W. Buschman, R.A. Washburn, Disassembly and Phase I Examination of EBR-II Superheater SU-712, Argonne National Laboratory Report ANL-82-16, 1982.
[3] K.J. Longua, D.L. Porter, R.G. Pahl, J.A. Buzzel, G.D. Hudman, Materials Examinations of the Components of EBR-II Superheater SU-712, Argonne National Laboratory Report ANL-83-103, 1984.
[4] J.M. Holt, H. Mindlin, C.Y. Ho (Eds.), Structural Alloys Handbook, 1996 Ed., CINDAS/Purdue University, 1997.
[5] K.J. Longua, Trans. ANS 38 (1981) 321.
[6] D.M. Wachs, D.D. Keiser, D.L. Porter, N. Kisohara, Nucl. Technol., submitted for publication.
[7] Y. Tomita, T. Kosugi, J. Kubota, K. Nakajima, T. Tsuchiya, Liquid Metal Engineering and Technology, Paper 145, BNES, London, 1984, p. 189.
[8] K. Roko, K. Takitani, A. Yoshizaki, M. Shiraha, in: Sixth International Heat Transfer Conference, Toronto, 1978, p. 429.
[9] T.C. Totemeier, Fatigue testing of metallurgically-bonded EBR-II superheater tubes, Idaho National Laboratory Report INL/EXT-06-12011, 2006.
[10] S. Suresh, Fatigue of Materials, Cambridge University, Cambridge, UK, 1991.
[11] W.F. Gale, T.C. Totemeier (Eds.), Smithells Metals Reference Book, 8th Ed., Elsevier/Butterworth-Heinemann, Oxford, UK, 2004, p. 11.
[12] H.H. Uhlig, R.W. Revie, Corrosion and Corrosion Control, 3rd Ed., John Wiley, New York, 1985.